ELSEVIER

Journal of Nuclear Materials 258–263 (1998) 1623–1627

journal of nuclear materials

Temperature dependence of bubble structure in 316L stainless steel irradiated with 2.5 MeV He ions [1]

C.H. Zhang [a,*], K.Q. Chen [a], Y.S. Wang [a], J.G. Sun [b]

[a] *Institute of Modern Physics, Academia Sinica, P.O. Box 31, Lanzhou 730000, People's Republic of China*
[b] *General Institute for Nonferrous Metals, Beijing, 100088, People's Republic of China*

Abstract

In this work, specimens of 316L stainless steel were implanted with 2.5 MeV He^+ ions at constant temperatures of 25°C, 200°C, 300°C, 400°C, 500°C, 550°C, and step-wise variant temperatures of 25°C/600°C and 300°C/550°C, respectively. The dose and dose rate were 2.5×10^{21}He ion/m^2 and 3.2–3.8 $\times 10^{16}$He ion/m^2/s for each implantation. Bubble structures were investigated with cross-section transmission electron microscopy (XTEM). The temperature dependence of the measured number density and mean size of bubbles exhibited two distinctly different regimes with a transition occurring at 300–400°C. The apparent activation energies suggest that bubble formation is controlled by diffusion of He atoms or He clusters in the high temperature regime, and by an athermal process in the low temperature regime. Cold working of the material had observable effects on bubble formation only in the high temperature regime. Under the varying temperature conditions, bubble formation was influenced strongly by the temperature of the first implantation, even if its dose was low. © 1998 Elsevier Science B.V. All rights reserved.

1. Introduction

The introduction of helium into metals can lead to formation of bubbles which would result in undesired changes of the metal properties, such as enhanced swelling [1] or high temperature embrittlement [2]. To understand mechanistically the formation behavior of helium bubbles in metals is of great interest for fusion energy engineering. For decades, considerable work has been done in pure Ni and stainless steels using helium implantation and subsequent microstructural investigation with electron microscopy, as reviewed by Singh and Trinkaus in Ref. [3]. The previous studies, however, have focused on the temperature range above 0.5 of the absolute melting point of the metals ($0.5T_m$), and fewer studies have been done in the technologically important range below $0.5T_m$ [3].

In the present work, we studied the formation of bubbles in 316L stainless steel at temperatures ranging from ambient temperature to 600°C (around $0.5T_m$ for stainless steels). Two types of treatment (i.e. with or without cold working) were carried out before implantation to investigate the influence of cold working of the material on bubble formation. In addition to the formation of bubbles under constant temperature conditions, effects of temperature variation on bubble structures were studied by changing temperature in a step-wise manner during helium implantation.

2. Experimental procedures

Austenitic 316L stainless steel, with a composition given in Table 1, was used in this study. Prior to implantation, two different types of treatment were performed: some specimens were solution-annealed at 1050°C for 1 h in a vacuum of 2 Pa, which are denoted as SA-type; and the others were cold worked by 20% after the same solution-annealing treatment, which are denoted as CW-type. Both types were well polished to a thickness of 0.3 mm.

* Corresponding author. Tel.: +86 0931 8854867; fax: +86 0931 8881100; e-mail: hiam@ns.lzb.ac.cn.

[1] Work is supported by the Hybrid Reactor Committee and the National Science Foundation of China.

0022-3115/98/$19.00 © 1998 Elsevier Science B.V. All rights reserved.
PII: S0022-3115(98)00332-8

Table 1
Composition of 316L stainless steel (wt%)

C	Si	P	S	Mn	Mo	Ni	Cr	Fe
0.025	0.29	0.017	0.015	1.41	2.25	14.14	17.22	Bal.

Implantation was performed with 2.5 MeV He^+ ions in a high-temperature target chamber connected to a 2×1.7 MV tandem accelerator in Peking University. Specimens were installed on a specimen holder which could be heated with built-in tungsten coils. The temperature was measured by a thermocouple fixed at the specimen surface. The beam current was measured with a hollow Faraday cup installed in front of the specimen holder.

Constant temperature implantations were performed at RT, 200°C, 300°C, 400°C, 500°C and 550°C, respectively. An SA and a CW specimen were implanted simultaneously at each temperature. The conditions for implantation were given in Table 2. In addition, two SA-type specimens were implanted under varying temperature conditions as described in Table 3. Each specimen was first implanted to a low-dose at a lower temperature, then implanted continuously at a higher temperature to a dose equal to that of the implantation under constant temperature condition. During implantation, the ion beam produced a uniform dose rate in a 5×5 mm^2 area on a specimen, and the increase of temperature induced by ion beam heating was below 20°C.

After implantation, specimens were electroplated with nickel in $NiCl_2/NiSO_4$ acid solution to become 3 mm in thickness, then were cut into cross-sectional foils. The cross-sectional foils were thinned by ion beam milling, then were investigated in a transmission electron microscope of JEM-200CX.

Since He concentration and displacement damage vary with depth for monoenergetic ion implantation, we here consider the microstructures at the peak-dose depth which is about 4 μm beneath the specimen surface for the implantation with 2.5 MeV He^+ ions. The corresponding values of helium concentration and displacements per atom (dpa) from TRIM calculation are given in Tables 2 and 3.

3. Results

Morphologies of bubbles formed under the constant temperature conditions are shown in Fig. 1 for SA-type, and in Fig. 2 for CW-type. Morphologies of bubbles formed under varying temperature conditions are shown in Fig. 3. The measured number density and mean diameter of bubbles are plotted in Fig. 4 as a function of implantation temperature.

In Fig. 4, the temperature dependence of both number density and mean diameter of bubbles exhibited two distinctly different regimes with a transition occurring between 300°C and 400°C: the bubble structure was independent of temperature below the border, while it changed sharply above the border. The presence of the two regimes indicate that the mechanism underlying bubble formation does not hold constant in the temperature range considered.

It is noticeable that pre-implantation cold working treatment of the material increased the number density and decreased the mean size of bubbles in the high temperature regime, while it had no observable effects in the low temperature regime, indicating that dislocations produced by the cold working ($\sim 10^{15}$ m^{-2} in density) have strong effects on bubble nucleation and growth only in the high temperature regime.

Table 2
Conditions for He implantation under constant temperatures. The maximum values of dpa and He concentration, C_{He}, refer to the peak-dose depth values calculated by TRIM-88 code (using $E_d = 45$ eV)

Temperature (°C)	Fluence (ions/m^2)	Flux (ions/m^2/s)	dpa (max)	C_{He} (max)(appm)
25,200,300,400,500,550 respectively	2.5×10^{21}	$3.2–3.8 \times 10^{16}$	10	9×10^4

Table 3
Conditions for He implantation under varying temperatures. The maximum values of dpa and He concentration, C_{He}, refer to the peak-dose depth values calculated by TRIM-88 code (using $E_d = 45$ eV).

Temperature (°C)	Fluence (ions/m^2)	Flux (ions/m^2/s)	dpa (max)	C_{He} (max)(appm)
300/550	6×10^{18} (at 300°C)	$3.2–3.8 \times 10^{16}$	0.02 (at 300°C)	2×10^2 (at 300°C)
	$+2.5 \times 10^{21}$ (at 550°C)		+10 (at 550°C)	$+9 \times 10^4$(at 550°C)
25/600	3×10^{19} (at 25°C)	$3.2–3.8 \times 10^{16}$	0.1 (at 25°C)	1×10^3 (at 25°C)
	$+2.5 \times 10^{21}$ (at 600°C)		+10 (at 600°C)	$+9 \times 10^4$(at 600°C)

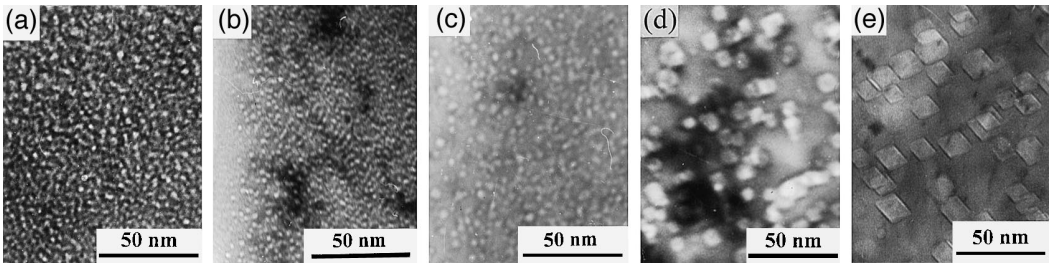

Fig. 1. Typical morphologies of bubbles at the peak-dose depth in SA-type specimens implanted at: (a) 25°C; (b) 300°C; (c) 400°C; (d) 500°C, and (e) 550°C.

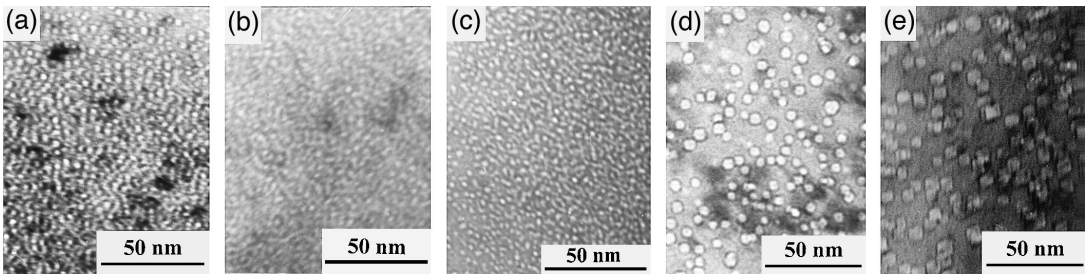

Fig. 2. Typical morphologies of bubbles at the peak-dose depth in CW-type specimens implanted at: (a) 25°C; (b) 200°C; (c) 300°C; (d) 500°C, and (e) 550°C.

It is also interesting that bubble structures formed under the varying temperature condition of 300°C/550°C were significantly different from those formed at a constant temperature of 550°C: the number density was increased significantly while the mean size was suppressed. This fact means that the first-step implantation has strong effects on bubble structures even if its dose is very low.

We get the mean values of apparent activation energies for the number density (C_B) and mean diameter ($\overline{D}_B$) of bubbles (in constant temperature conditions) as follows when fitting the different branches in Fig. 4 to an Arrhenius behavior.

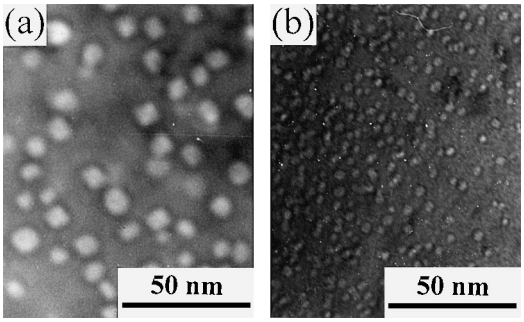

Fig. 3. Typical morphologies of bubbles at the peak-dose depth in SA-type specimens implanted under varying temperature conditions of (a) 25°C/600°C, and (b) 300°C/550°C.

In the high temperature regime

$$E^{\mathrm{act}}_{C_B} = 1.0\ \mathrm{eV}, \quad E^{\mathrm{act}}_{\overline{D}_B} = 0.37\ \mathrm{eV}. \tag{1}$$

In the low temperature regime

$$E^{\mathrm{act}}_{C_B}, E^{\mathrm{act}}_{\overline{D}_B} \approx 0. \tag{2}$$

4. Discussion

4.1. Bubble formation under constant temperature condition

According to the previous studies [3,4], small He clusters were expected to dissociate before trapping additional He atoms, and only those above a critical size can possibly survive at high temperature. In this case bubble formation is thermal He-resolution controlled (i.e. muti-atomic nucleation). On the other hand, even small He clusters were expected to be stable (i.e. diatomic nucleation) at lower temperatures so that the evolving bubble structure will be controlled by diffusion of either He atoms or He-atom clusters. The transition between the two temperature regimes occurs generally around $0.5T_m$ [3]. For irradiation-enhanced helium diffusion, there are two typical mechanisms: (1) the vacancy mechanism with the effective He diffusion coefficient $D_v c_v$ [5], and (2) the self-interstitial/He replacement mechanism with the effective He diffusion

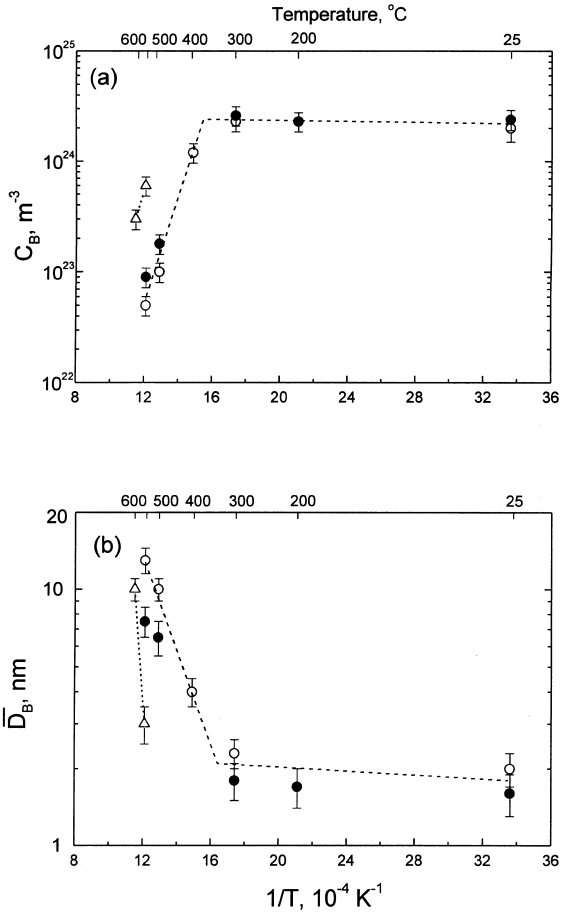

Fig. 4. Temperature dependence of (a) number density and (b) mean effective diameter of bubbles at the peak-dose depth in all specimens (Arrhenius plot). The open symbols, ○, refer to data points of SA-type specimens, and the full symbols, ●, refer to data points of CW-type specimens under the constant temperature conditions. The symbols Δ refer to data under the varying temperature conditions as a function of temperature of the second-step implantation.

coefficient D_v [6,7]; where D_v and c_v are the diffusivity and concentration of vacancies, respectively. The dependence of bubble density and mean size on temperature (apparent activation energy E^{act}) for various limiting cases has been summarized by Zell et al. in Ref. [8].

In the high temperature regime, the apparent activation energy of C_B (1.0 eV) given in Eq. (1) is much smaller than the dissociation energy of a He-vacancy (2.4 eV in Ni [9]), indicating that the bubble formation is not controlled by thermal resolution of He atoms from bubble nuclei. In Eq. (1), the apparent activation energy for $\overline{D}_B$ is nearly $\frac{1}{3}$ of that of C_B, indicating that the helium state within bubbles is in constant density [8]. The apparent activation energies given in Eq. (1) are substantially higher than theoretical values for He diffusion through the vacancy mechanism (corresponding to $E^{act}_{C_B} = -3E^M_V/14$ and $E^{act}_{\overline{D}_B} = E^M_V/14$, where E^M_V is activation energy for vacancy migration, 1.1–1.3 eV in SS). The self-interstitial/He replacement mechanism with higher apparent activation energies ($E^{act}_{C_B} = -3E^M_V/7$ and $E^{act}_{\overline{D}_B} = E^M_V/7$) is thus a more possible mechanism controlling bubble formation. Our C_B data are also in reasonable agreement with absolute values expected for the replacement mechanism, since they lie between the value of $2C^*_B$ (C^*_B is bubble density resulting from the early nucleation peak [3]) and 10-fold this value. He diffusion via the self-interstitial/He replacement mechanism has been identified to control bubble formation in low-dose He-irradiated Ni [8].

We mention here that our $E^{act}_{C_B}$ data is in good agreement with the values (1 eV for C_B in SS) resulting from the previous low-dose helium implantation in the same temperature range, as compiled in Ref. [3]. However, the activation energy for mono-vacancy migration deduced from the values in Eq. (1) by following Ref. [8] becomes about 2.5 eV and is roughly two times larger than commonly accepted values of free vacancy migration energy in 316L SS (1.1–1.3 eV). This discrepancy may imply that bubble formation was controlled by the diffusion of both atomic He and He clusters, since including the migration and coalescence of He clusters in rate equations would result in lower bubble density, larger bubble size and higher apparent activation energies [10].

In the low temperature regime, the bubble structures are likely to be independent of implantation temperature, and the very small apparent activation energies for both C_B and $\overline{D}_B$ indicate that there is an athermal mechanism controlling bubble formation. He diffusion with a high activation energy, such as the vacancy mechanism or the replacement mechanism, cannot be operative. He diffusion via the interstitial mechanism with a very low activation energy (~0.15eV in SS [11]) may be impeded strongly by highly dispersed vacancies. According to recent experimental work by Donnelly et al. [12], during Ar-ion irradiation He bubbles undergo athermal migration and coalescence in Au as a result of the interaction of bubbles with adjacent cascades. Since the present implantation with 2.5 MeV He ions produced ~10 dpa at the peak-dose depth, the athermal migration and coalescence of He clusters or bubbles induced by cascades may limit effectively the bubble density to moderate values.

A similar plateau feature in the temperature dependence of bubble structures was found previously in He-implanted Mo [13] and Kr-implanted Zr [14] as investigated with TEM, while the transition point of the two regimes moved up to 700°C in Mo, and 500°C in Zr. In general, the transition occurs around $0.35T_m$ for the three different materials.

4.2. Bubble formation under varying temperature condition

The number density of bubbles formed in the varying temperature condition of 300°C/550°C was over one order of magnitude higher than that formed at the constant temperature of 550°C, while only three times lower than that formed at the constant temperature of 300°C. This indicated that, first, the first low-dose implantation at 300°C led to the formation of small He clusters with high density; second, the small He clusters (each containing several He atoms) formed by the first implantation are thermally stable, and a considerable portion continue to be nuclei for the growth of bubbles in the subsequent implantation at 550°C thus greatly enhancing the bubble density.

Since the temperature of structural materials in fusion reactors is expected to fluctuate frequently depending on the operating conditions, studies on the microstructural evolution under varying temperature condition are of technological importance and more studies are needed.

5. Conclusions

The temperature dependence of the measured number density and mean size of He bubbles in 316L stainless steel which was helium implanted at temperatures ranging from 25°C to 550°C exhibited two distinctly different regimes with a transition occurring at 300–400°C. The apparent activation energies suggest that bubble formation is controlled by diffusion of He atoms or He clusters in the high temperature regime, and by an athermal process in the low temperature regime. Cold working of the material has observable effects on bubble formation only in the high temperature regime.

Under varying temperature conditions, bubble formation was influenced strongly by temperature of first-step implantation, even if its dose was low.

References

[1] K. Farrell, P.J. Maziasz, E.H. Lee, L.K. Mansur, Radiat. Eff. 78 (1983) 277.
[2] H. Ullmaier, Radiat. Eff. 78 (1983) 1.
[3] B.N. Singh, H. Trinkaus, J. Nucl. Mater. 186 (1992) 153.
[4] H. Trinkaus, J. Nucl. Mater. 133&134 (1985) 105; Radiat. Eff. 101 (1986) 91.
[5] A.J.E. Forman, B.N. Singh, J. Nucl. Mater. 141–143 (1986) 672.
[6] N.M. Ghoniem, S. Sharafat, J.M. Williams, L.K. Mansur, J. Nucl. Mater. 117 (1983) 96.
[7] H. Trinkaus, J. Nucl. Mater. 118 (1983) 39.
[8] V. Zell, H. Schroeder, H. Trinkaus, J. Nucl. Mater. 212–215 (1994) 358.
[9] V. Philipps, K. Sonnenberg, J.M. Williams, J. Nucl. Mater. 107 (1982) 271.
[10] M. Fell, S.M. Murphy, J. Nucl. Mater. 172 (1990) 1.
[11] F. Carsughi, Investigations on helium bubble structure in metals by neutron scattering and electron microscopy, Degree Thesis, Jül-2652, Institut für FestkÖrperforschung, Jülich, Germany, 1992.
[12] S.E. Donnelly, R.C. Birtcher, C. Templier, V. Vishnyakov, Phys. Rev. B 52 (1995) 3970.
[13] D.J. Mazey, B.L. Eyre, J.H. Evans, S.K. Erents, G.M. McCracken, J. Nucl. Mater. 64 (1977) 145.
[14] J.H. Evans, in: S.E. Donnelly, J.H. Evans (Eds.), Fundamental Aspects of Inert Gases in Solids, Plenum Press, New York, 1991, p. 307.